Available online at www.sciencedirect.com
ScienceDirect
Journal of Solid State Chemistry 180 (2007) 956–967
JOURNAL OF SOLID STATE CHEMISTRY
www.elsevier.com/locate/jssc

Crystal chemistry of $M[PO_2(OH)_2]_2 \cdot 2H_2O$ compounds (M = Mg, Mn, Fe, Co, Ni, Zn, Cd): Structural investigation of the Ni, Zn and Cd salts

Violeta Koleva[a], Herta Effenberger[b,*]

[a]*Institute of General and Inorganic Chemistry, Bulgarian Academy of Sciences, Acad. G. Bonchev St., Bl.11, 1113 Sofia, Bulgaria*
[b]*Institut für Mineralogie und Kristallographie, Universität Wien, Althanstraße 14, A-1090 Wien, Austria*

Received 27 September 2006; received in revised form 22 December 2006; accepted 26 December 2006
Available online 7 January 2007

Abstract

The compounds $M[PO_2(OH)_2]_2 \cdot 2H_2O$ (M = Mg, Mn, Fe, Co, Ni, Zn, Cd) were prepared from super-saturated aqueous solutions at room temperature. Single-crystal X-ray structure investigations of members with M = Ni, Zn, Cd were performed at 295 and 120 K. The space-group symmetry is $P2_1/n$, $Z = 2$. The unit-cell parameters are at 295/120 K for M = Ni: $a = 7.240(2)/7.202(2)$, $b = 9.794(2)/9.799(2)$, $c = 5.313(1)/5.285(1)$ Å, $\beta = 94.81(1)/94.38(1)^\circ$, $V = 375.4/371.9$ Å^3; M = Zn: $a = 7.263(2)/7.221(2)$, $b = 9.893(2)/9.899(3)$, $c = 5.328(1)/5.296(2)$ Å, $\beta = 94.79(1)/94.31(2)^\circ$, $V = 381.5/377.5$ Å^3; M = Cd: $a = 7.356(2)/7.319(2)$, $b = 10.416(2)/10.423(3)$, $c = 5.407(1)/5.371(2)$ Å, $\beta = 93.85(1)/93.30(2)^\circ$, $V = 413.4/409.1$ Å^3. Layers of corner-shared MO_6 octahedra and phosphate tetrahedra are linked by three of the four crystallographically different hydrogen bonds. The fourth hydrogen bond (located within the layer) is worth mentioning because of the short $O_h \cdots O$ bond distance of 2.57–2.61 Å at room temperature (2.56–2.57 Å at 120 K); only for M = Mg it is increased to 2.65 Å. Any marked temperature-dependent variation of the unit-cell dimension is observed only vertical to the layers. The analysis of the infrared (IR) spectroscopy data evidences that the internal PO_4 vibrations are insensitive to the size and the electronic configuration of the M^{2+} ions. The slight strengthening of the intra-molecular P–O bonds in the Mg salt is caused by the more ionic character of the Mg–O bonds. All IR spectra exhibit the characteristic "*ABC* trio" for acidic salts: 2900–3180 cm^{-1} (*A* band), 2000–2450 cm^{-1} (*B* band) and 1550–1750 cm^{-1} (*C* band). Both the frequency and the intensity of the *A* band provide an evidence that the $PO_2(OH)_2$ groups in $M[PO_2(OH)_2]_2 \cdot 2H_2O$ compounds form weaker hydrogen bonds as compared with other acidic salts with comparable $O \cdots O$ bond distances of about 2.60 Å. The observed shift of the O–H stretching vibrations of the water molecule in the order M = Mg > Mn ≈ Fe ≈ Co > Ni > Zn ≈ Cd has been discussed with respect to the influence of both the character and the strength of $M \leftrightarrow H_2O$ interactions.

Keywords: $M[PO_2(OH)_2]_2 \cdot 2H_2O$ compounds; Diprotonated phosphates; Crystal structure; Low-temperature measurement; IR spectroscopy

1. Introduction

Compounds with the general formula $M[PO_2(OH)_2]_2 \cdot 2H_2O$ have been investigated extensively during the last decades. The crystal structure was determined for Cd $[PO_2(OH)_2]_2 \cdot 2H_2O$ first [1]. Isotypy with $Zn[PO_2(OH)_2]_2 \cdot 2H_2O$ was mentioned based on the comparison of unit-cell parameters and X-ray powder patterns [2]. Later on, accurate single-crystal structural investigations of the Mg, Mn, Fe and Co members were performed [3–6]. For early syntheses of these compounds which in parts date back to the second half of the 19th century, see the references in the literature mentioned above.

In connection with investigations of the coordination chemistry of transition-metal atoms towards O atoms, we aimed to compare the crystal chemistry of *di*protonated phosphates $M[PO_2(OH)_2]_2 \cdot 2H_2O$. Due to the fact that the H atoms were not located in the Cd compound [1] and no structural data for the Ni and Zn compound have been available, appropriate crystals were synthesized and investigated by single-crystal X-ray diffraction techniques. In order to gain detailed insights into the crystal chemistry

*Corresponding author. Fax: +43 1 4277 53249.
E-mail addresses: vkoleva@svr.igic.bas.bg (V. Koleva), herta.silvia.effenberger@univie.ac.at (H. Effenberger).

0022-4596/$ - see front matter © 2007 Elsevier Inc. All rights reserved.
doi:10.1016/j.jssc.2006.12.024

of the $M[PO_2(OH)_2]_2 \cdot 2H_2O$-type compounds, their infrared (IR) spectra were recorded for the discussion of the hydrogen bonding.

2. Experimental

2.1. Synthesis

Single crystals of $Cd[PO_2(OH)_2]_2 \cdot 2H_2O$ were obtained from a super-saturated aqueous solution containing 8.5 wt% CdO and 56 wt% H_3PO_4; it was slowly cooled from about 70 °C to room temperature (a cooling rate of about 10 °C h^{-1} was used). Single crystals of both the Zn and Ni salts were prepared from solutions containing 13 wt% ZnO + 62 wt% H_3PO_4, and 9 wt% NiO (the corresponding amount of $NiCO_3$ was dissolved) + 70 wt% H_3PO_4, respectively. Slow concentration at room temperature was allowed in a desiccator over silica. A few $Cd[PO_2(OH)_2]_2 \cdot 2H_2O$ crystals were added as seed crystals in both solutions. Without nuclei initializing the crystallization, single crystals were not observed even after more than 2 months. Lath-like single crystals of $Zn[PO_2(OH)_2]_2 \cdot 2H_2O$ were obtained after about a month. The size of the crystals is up to 0.2 mm in length and 0.1 mm in diameter. As a by-product, needle to lath-like crystals of $Zn_3[PO_3(OH)]_3 \cdot 3H_2O$ [7] were obtained.

In the case of the Ni salt, only a few and very small crystals appeared after 1 month; consequently, the experimental conditions were changed: the silica was removed to prevent any further concentration of the mother liquor. Thus, the crystals already obtained increased in size. However, they were much smaller as compared to those of the other compounds (maximum size $0.04 \times 0.06 \times 0.12\,mm^3$).

The powder-like samples of the Mg, Mn, Fe and Co salts were synthesized from acidic phosphate solutions containing 5–9 wt% metal oxide and 65 wt% H_3PO_4 by a salting out procedure with acetone for the Mg salt and ethyl alcohol for the other salts. Metal carbonates of Mn^{2+} and Co^{2+}, MgO, and a powder of native Fe were used for the preparation of the solutions. The synthesis of the Fe salt was performed in an argon atmosphere (99.999 wt%) in order to prevent the oxidation of Fe^{2+}. All reagents used for the syntheses were of "p.a." quality. The powder samples thus obtained were identified and checked for purity with respect to other phases by X-ray powder-diffraction techniques and chemical analyses for the M^{2+} concentrations.

2.2. Crystal structure investigation

Single-crystal X-ray data collections at room temperature and at 120 K were performed on small crystal chips of the compounds $M[PO_2(OH)_2]_2 \cdot 2H_2O$, with M = Ni, Zn and Cd. Details on the data collection are compiled in Table 1. The atomic coordinates of $Co[PO_2(OH)_2]_2 \cdot 2H_2O$ [6] served in the starting set for the structure refinements. Space-group symmetry $P2_1/n$ was confirmed for all substances; it is the setting of the reduced cell. Also, the low-temperature measurements did not show any evidence for a phase transition. Anisotropic displacement parameters were allowed to vary for the M, P and O atoms; for the H atoms only isotropic displacement parameters were refined. The highest peaks in the final difference Fourier maps are located along the P–O bonds, they reflect the pronounced covalent bond character within the phosphate groups. Final structure parameters are given in Table 2. Atom labelling is consistent with that given in the original papers of the compounds with M = Mg, Fe, and Co [3,5,6]. In the paper of $Mn[PO_2(OH)_2]_2 \cdot 2H_2O$ an interchanged labelling for the atom pairs O1 and O2 as well as O_h3 and O_h4 was used [4]. To enable the crystal chemical comparison of $M[PO_2(OH)_2]_2 \cdot 2H_2O$ compounds, the labelling is adopted throughout the present paper; so all atoms O1, O2, O_h3, O_h4 and O_w5 refer topologically to the same atom site in the relevant phase. Interatomic bond distances and bond angles are given in Table 3. The differences of the atomic sites of $Cd[PO_2(OH)_2]_2 \cdot 2H_2O$ given in the earlier paper [1] and those of the present refinement are 0.005 Å for the P atom and up to 0.025 Å for the O atoms.

The crystallographic files in cif format for $M[PO_2(OH)_2]_2 \cdot 2H_2O$, M = Ni, Zn and Cd have been deposited with FIZ Karlsruhe as CSD numbers 417429, 417431 and 417427 (295 K) and 417430, 417432 and 417428 (120 K). These data may be obtained by contacting FIZ Karlsruhe at +49 7247 808 666 (fax) or crysdata@fiz-karlsruhe.de (e-mail).

2.3. IR spectroscopic investigation

The IR spectra were recorded at room temperature on a Bruker model IRS 113v Fourier transform interferometer (resolution $<2\,cm^{-1}$). KBr discs were used for the Mg, Mn, Fe, Co and Ni salts (4000–350 cm^{-1}) but nujol (1400–350 cm^{-1}) and fluorolube (4000–1400 cm^{-1}) mulls for the Zn and Cd salts.

3. Results and discussion

Throughout this paper, all crystal chemical data of the $M[PO_2(OH)_2]_2 \cdot 2H_2O$ compounds with M = Mg, Mn, Fe and Co used for comparison with the structure investigations performed during the present work refer to Refs. [3–6]. The type structure of the $M[PO_2(OH)_2]_2 \cdot 2H_2O$ compounds (M = Mg, Mn, Fe, Co, Ni, Zn and Cd) is characterized by isolated $MO_4(O_w)_2$ octahedra with site symmetry $\bar{1}$ and *di*protonated phosphate groups. The octahedra are formed by four O atoms representing each a corner of a phosphate tetrahedron; they are completed by two oxygen atoms belonging to water molecules (O_w atoms). Vice versa, the $PO_2(OH)_2$ groups link each of two MO_6 octahedra to form $M[PO_2(OH)_2]_2(H_2O)_2$ layers parallel to $(\bar{1}01)$ (Fig. 1a,b). The network –*M*–O–P– deviates only slightly from coplanarity. The O_w and O_h

Table 1
Single-crystal X-ray data collection and structure refinements of $M[PO_2(OH)_2]_2 \cdot 2H_2O$ compounds (M = Ni, Zn, Cd); space group $P2_1/n$; $Z = 2$

$M[PO_2(OH)_2]_2 \cdot 2H_2O$	M = Ni		M = Zn		M = Cd	
Temperature (K)	295	120	295	120	295	120
a (Å)	7.240(2)	7.202(2)	7.263(2)	7.221(2)	7.356(2)	7.319(2)
b (Å)	9.794(2)	9.799(2)	9.893(2)	9.899(3)	10.416(2)	10.423(3)
c (Å)	5.313(1)	5.285(1)	5.328(1)	5.296(2)	5.407(1)	5.371(2)
β (°)	94.81(1)	94.38(1)	94.79(1)	94.31(2)	93.85(1)	93.30(2)
V (Å^3)	375.4	371.9	381.5	377.5	413.4	409.1
ρ_{calc} (g cm^{-3})	2.55	2.58	2.57	2.60	2.75	2.78
Crystal dimensions (μm)	35 × 60 × 115	35 × 60 × 115	60 × 70 × 90	60 × 70 × 90	70 × 80 × 120	70 × 80 × 120
Range of data collection (deg)	$3<2\vartheta<70$	$3<2\vartheta<70$	$3<2\vartheta<70$	$3<2\vartheta<70$	$3<2\vartheta<70$	$3<2\vartheta<70$
Number of images	553	326	636	414	601	324
Scan time (s deg^{-1})	85	130	105	100	45	60
Measured reflections	6362	6035	6366	6266	7075	6773
$R_{int} = \Sigma\lvert F_o^2 - F_o^2(\text{mean})\rvert / \Sigma F_o^2$	0.024	0.026	0.027	0.031	0.023	0.025
μ(Mo$K\alpha$) (mm^{-1})	3.1	3.1	3.7	3.7	3.1	3.1
Extinction parameter	0.029(4)	0.041(5)	0.042(2)	0.015(2)	0.0208(12)	0.0118(12)
$R1 = \Sigma(\lvert\lvert F_o\rvert - \lvert F_c\rvert\rvert)/\Sigma F_o$	0.026	0.024	0.020	0.019	0.017	0.016
$wR2 = [\Sigma w(F_o^2 - F_c^2)^2 / \Sigma \lvert wF_o^4\rvert]^{1/2}$	0.074	0.066	0.050	0.048	0.044	0.042
Unique reflections (n)	1648	1630	1669	1659	1821	1800
Reflections with $F_o > 4\Sigma(F_o)$	1474	1490	1451	1480	1630	1676
GooF $= \Sigma[w(F_o^2 - F_c^2)^2]/(n-p)^{0.5}$	1.08	1.04	1.12	1.06	0.92	0.98
P_1	0.048	0.039	0.023	0.020	0.025	0.022
P_2	0.07	0.18	0.07	0.16	0.32	0.21
max Δ/σ	⩽0.001	⩽0.001	⩽0.001	⩽0.001	⩽0.001	⩽0.001
Final difference Fourier map (e Å^{-3})	−0.77 to +0.49	−0.62 to +0.53	−0.41 to +0.54	−0.43 to +0.53	−0.53 to +0.82	−0.55 to +0.55

NONIUS four-circle diffractometer equipped with a CCD detector and a fiber optics collimator, Mo tube, graphite monochromator, scan modes: φ scans for distinct ω angles (room-temperature measurements) and ω scans at $\chi = 55°$ (low-temperature measurements), rotation angle for each image 2°, frame size: binned mode, 621 × 576 pixels, detector-to-sample distance: 30 mm; range of data collection: $\pm h \pm k \pm l$. Unit-cell parameters were obtained by least-squares refinements of accurate 2ϑvalues. Corrections for Lorentz, polarization and absorption effects (multi-scan method); neutral-atomic complex scattering functions [8]; program SHELXL-97 [9].
$w = 1/\sigma^2(F_o^2) + [P_1 \times P]^2 + P_2 \times P$; $P = ([\max(0, F_o^2)] + 2 \times F_c^2)/3]$; number of variable parameters (p) is 78.

atoms lie off the layer. The corners of the phosphate tetrahedron not linked with the M atoms represent the hydroxyl groups (O_h atoms). Topologically, the layers consist of eight-membered rings built from each four $MO_4(O_w)_2$ octahedra and four $PO_2(OH)(O_h)_2$ groups. Both hydrogen bonds of the water molecule have the acceptor atoms in a neighbouring layer (O_w5–$H_w1\cdots O2$ and O_w5–$H_w2\cdots O_h4$). One of the hydrogen bonds of the hydroxyl groups is within the layer (O_h4–$H_h4\cdots O1$) whereas the other one links to a neighbouring layer (O_h3–$H_h3\cdots O_w5$).

3.1. Unit-cell metrics

The unit-cell parameters a, b and c as well as the unit-cell volume correlate positively with the ionic radii of the M atoms whereas the angle β decreases (Fig. 2). Comparing the results of the room- and low-temperature data, it is obvious that the unit-cell parameter b is practically invariant; it varies only within three standard deviations. For the interpretation of the temperature-controlled compression behaviour, a transformation of the unit cell according to $(101/010/10\bar{1})$ is worthwhile. This causes the space-group setting $P2_1/a$. Both directions $a[P2_1/a]$ and $b[P2_1/a] = b[P2_1/n]$ are within the $M[PO_2(OH)_2]_2(H_2O)_2$ layer; their axial lengths taken at 120 and 295 K are practically maintained. Consequently, the $M[PO_2(OH)_2]_2$ $(H_2O)_2$ layers have to be considered as more or less invariant with respect to their translation periods within the range of temperature investigated. In contrast, $c[P2_1/a]$ inclines with respect to the $M[PO_2(OH)_2]_2(H_2O)_2$ layer and exhibits a strong temperature depending compression behaviour. Only the hydrogen-bond lengths depend on the temperature markedly. The angle $\beta[P2_1/a]$ scatters within ~0.3°. The variation in the monoclinic angle observed for the $P2_1/n$ setting is a result of the anisotropic compression behaviour of the title compounds only. The shift of succeeding layers is maintained within this series of compounds.

3.2. MO_6 octahedra

As expected, the $MO_4(O_w)_2$ octahedra differ in their size with respect to the ionic radii of the M atoms (see Fig. 3a). The individual M–O and M–O_w bond lengths scatter moderately; the largest differences were found for M = Fe. Worth mentioning is that the smallest difference observed within the whole series occurs for M = Co. *D*ivalent Co atoms have an electron configuration [Ar]$3d^7$; consequently, a distortion in an octahedral complex is possible

Table 2
Fractional atomic coordinates and displacement parameters

	x	y	z	U_{equiv}/U_{iso}	U_{11}	U_{22}	U_{33}	U_{23}	U_{13}	U_{12}
$Ni[PO_2(OH)_2]_2 \cdot 2H_2O$, 295 K										
Ni	0.5000	0.5000	0.5000	0.01194(8)	0.01217(12)	0.01088(11)	0.01254(12)	0.00007(6)	−0.00041(7)	−0.00019(6)
P	0.83704(4)	0.28519(3)	0.74293(6)	0.01240(9)	0.01218(14)	0.01198(14)	0.01255(14)	−0.00034(9)	−0.00182(10)	0.00099(9)
O1	0.64425(13)	0.33263(10)	0.65435(19)	0.0175(2)	0.0143(4)	0.0159(4)	0.0213(4)	0.0017(3)	−0.0045(3)	0.0009(3)
O2	0.86181(14)	0.13231(9)	0.73744(18)	0.0178(2)	0.0225(4)	0.0133(4)	0.0164(4)	−0.0014(3)	−0.0043(3)	0.0036(3)
O_h3	0.97029(16)	0.35565(13)	0.5651(2)	0.0249(2)	0.0197(5)	0.0313(6)	0.0238(5)	0.0050(4)	0.0015(4)	−0.0077(4)
O_h4	0.88638(15)	0.33946(10)	0.0183(2)	0.0216(2)	0.0257(5)	0.0209(4)	0.0166(4)	−0.0060(3)	−0.0068(3)	0.0085(4)
O_w5	0.30311(13)	0.46380(11)	0.7551(2)	0.0166(2)	0.0171(4)	0.0170(4)	0.0160(4)	0.0010(3)	0.0021(3)	0.0010(3)
H_w1	0.343(4)	0.427(3)	−0.105(5)	0.016(6)						
H_w2	0.269(4)	0.539(3)	0.797(6)	0.017(7)						
H_h3	0.054(4)	0.368(3)	0.609(6)	0.024(8)						
H_h4	0.985(5)	0.282(4)	0.107(7)	0.040(10)						
$Ni[PO_2(OH)_2]_2 \cdot 2H_2O$, 120 K										
Ni	0.5000	0.5000	0.5000	0.00719(8)	0.00711(11)	0.00682(11)	0.00755(11)	0.00008(6)	−0.00006(7)	−0.00005(6)
P	0.83767(4)	0.28512(3)	0.74203(5)	0.00753(8)	0.00730(13)	0.00740(13)	0.00771(13)	−0.00022(9)	−0.00071(9)	0.00024(8)
O1	0.64365(12)	0.33247(9)	0.65455(17)	0.01023(16)	0.0082(3)	0.0097(3)	0.0125(4)	0.0006(3)	−0.0017(3)	−0.0002(3)
O2	0.86239(12)	0.13193(9)	0.73557(16)	0.01021(15)	0.0118(4)	0.0082(3)	0.0103(3)	−0.0005(3)	−0.0014(3)	0.0009(3)
O_h3	0.97212(13)	0.35609(10)	0.56320(18)	0.01288(16)	0.0102(4)	0.0154(4)	0.0129(4)	0.0018(3)	0.0005(3)	−0.0037(3)
O_h4	0.88630(13)	0.33874(9)	0.01984(17)	0.01191(16)	0.0134(4)	0.0119(4)	0.0098(3)	−0.0026(3)	−0.0029(3)	0.0036(3)
O_w5	0.30103(12)	0.46373(9)	0.75530(17)	0.00987(15)	0.0097(3)	0.0101(4)	0.0098(3)	0.0001(3)	0.0007(3)	0.0011(3)
H_w1	0.342(3)	0.422(3)	−0.099(5)	0.005(5)						
H_w2	0.264(4)	0.540(3)	0.790(5)	0.008(6)						
H_h3	0.063(4)	0.370(2)	0.617(5)	0.006(6)						
H_h4	0.987(7)	0.281(5)	0.124(9)	0.072(15)						
$Zn[PO_2(OH)_2]_2 \cdot 2H_2O$, 295 K										
Zn	0.5000	0.5000	0.5000	0.01230(6)	0.01284(10)	0.01048(10)	0.01335(9)	0.00003(6)	−0.00031(6)	−0.00055(6)
P	0.83715(4)	0.28527(3)	0.74355(5)	0.01127(7)	0.01142(13)	0.01025(13)	0.01159(12)	−0.00033(9)	−0.00224(9)	0.00086(9)
O1	0.64493(12)	0.33251(9)	0.65757(17)	0.01633(16)	0.0122(4)	0.0142(4)	0.0214(4)	0.0016(3)	−0.0052(3)	0.0011(3)
O2	0.86201(13)	0.13396(8)	0.73591(16)	0.01670(17)	0.0229(4)	0.0108(4)	0.0153(4)	−0.0014(3)	−0.0049(3)	0.0037(3)
O_h3	0.96905(15)	0.35616(12)	0.5668(2)	0.0247(2)	0.0194(5)	0.0315(6)	0.0231(4)	0.0044(4)	0.0010(4)	−0.0090(4)
O_h4	0.88711(14)	0.33820(10)	0.01834(17)	0.02076(19)	0.0246(5)	0.0204(4)	0.0158(4)	−0.0067(3)	−0.0071(3)	0.0090(3)
O_w5	0.29939(12)	0.46353(10)	0.75869(16)	0.01590(16)	0.0169(4)	0.0160(4)	0.0150(4)	0.0011(3)	0.0022(3)	0.0015(3)
H_w1	0.338(3)	0.425(2)	−0.106(4)	0.011(5)						
H_w2	0.262(3)	0.539(3)	0.803(4)	0.013(6)						
H_h3	0.046(3)	0.370(3)	0.617(4)	0.016(7)						
H_h4	0.980(6)	0.283(4)	0.127(7)	0.092(14)						
$Zn[PO_2(OH)_2]_2 \cdot 2H_2O$, 120 K										
Zn	0.5000	0.5000	0.5000	0.00588(6)	0.00602(8)	0.00532(9)	0.00624(8)	0.00011(5)	0.00005(5)	−0.00020(5)
P	0.83761(4)	0.28518(3)	0.74229(5)	0.00566(6)	0.00563(11)	0.00536(12)	0.00581(11)	−0.00020(9)	−0.00086(8)	0.00031(8)
O1	0.64394(11)	0.33250(8)	0.65779(16)	0.00850(14)	0.0066(3)	0.0078(4)	0.0107(3)	0.0009(3)	−0.0019(3)	0.0005(3)
O2	0.86250(11)	0.13358(8)	0.73355(15)	0.00835(14)	0.0109(3)	0.0057(3)	0.0081(3)	−0.0008(3)	−0.0016(3)	0.0015(3)
O_h3	0.97106(12)	0.35655(9)	0.56449(17)	0.01133(16)	0.0092(3)	0.0144(4)	0.0104(3)	0.0019(3)	0.0006(3)	−0.0040(3)
O_h4	0.88671(12)	0.33720(9)	0.02021(16)	0.01008(15)	0.0118(4)	0.0101(4)	0.0078(3)	−0.0025(3)	−0.0031(3)	0.0041(3)
O_w5	0.29711(11)	0.46369(9)	0.75868(15)	0.00824(14)	0.0088(3)	0.0079(3)	0.0081(3)	0.0002(3)	0.0011(3)	0.0008(3)
H_w1	0.340(3)	0.426(2)	−0.097(4)	0.000(5)						
H_w2	0.259(3)	0.537(2)	0.801(4)	0.000(5)						
H_h3	0.060(3)	0.373(2)	0.621(4)	0.005(6)						
H_h4	0.970(3)	0.290(3)	0.109(5)	0.016(6)						
$Cd[PO_2(OH)_2]_2 \cdot 2H_2O$, 295 K										
Cd	0.5000	0.5000	0.5000	0.01333(5)	0.01459(7)	0.01043(6)	0.01463(7)	0.00006(3)	−0.00169(4)	−0.00069(4)
P	0.83337(4)	0.28388(3)	0.74712(6)	0.01343(7)	0.01397(13)	0.01153(12)	0.01411(13)	0.00009(10)	−0.00415(9)	0.00124(10)
O1	0.64093(13)	0.32540(10)	0.6745(2)	0.0199(2)	0.0152(4)	0.0159(4)	0.0273(5)	0.0025(4)	−0.0081(3)	0.0018(3)
O2	0.86477(15)	0.14170(10)	0.7229(2)	0.0202(2)	0.0289(5)	0.0130(4)	0.0176(4)	−0.0009(3)	−0.0067(4)	0.0057(4)
O_h3	0.95811(17)	0.36162(13)	0.5777(2)	0.0286(2)	0.0248(5)	0.0336(6)	0.0270(5)	0.0068(5)	−0.0023(4)	−0.0109(5)
O_h4	0.88153(15)	0.32736(11)	0.0219(2)	0.0233(2)	0.0276(5)	0.0226(5)	0.0183(4)	−0.0066(4)	−0.0085(4)	0.0102(4)
O_w5	0.27617(14)	0.46267(11)	0.775(2)	0.01832(18)	0.0200(4)	0.0177(4)	0.0174(4)	0.0012(3)	0.0023(3)	0.0010(3)
H_w1	0.317(3)	0.425(3)	−0.097(5)	0.013(6)						
H_w2	0.241(4)	0.532(3)	0.815(5)	0.011(6)						
H_h3	0.039(4)	0.376(3)	0.634(5)	0.018(7)						
H_h4	0.964(4)	0.281(3)	0.104(5)	0.028(8)						

Table 2 (*continued*)

	x	*y*	*z*	U_{equiv}/U_{iso}	U_{11}	U_{22}	U_{33}	U_{23}	U_{13}	U_{12}
$Cd[PO_2(OH)_2]_2 \cdot 2H_2O$, 120 K										
Cd	0.5000	0.5000	0.5000	0.00617(4)	0.00674(6)	0.00480(6)	0.00684(6)	0.00002(3)	−0.00069(4)	−0.00031(3)
P	0.83330(4)	0.28369(3)	0.74606(5)	0.00661(6)	0.00702(11)	0.00548(11)	0.00709(12)	−0.00003(9)	−0.00176(8)	0.00048(8)
O1	0.63945(11)	0.32520(8)	0.67479(17)	0.00968(15)	0.0076(3)	0.0079(3)	0.0132(4)	0.0013(3)	−0.0032(3)	0.0008(3)
O2	0.86499(12)	0.14112(8)	0.72068(16)	0.00973(15)	0.0138(4)	0.0064(3)	0.0086(4)	−0.0002(3)	−0.0028(3)	0.0022(3)
O_h3	0.95922(13)	0.36192(9)	0.57566(18)	0.01297(16)	0.0114(4)	0.0150(4)	0.0123(4)	0.0030(3)	−0.0009(3)	−0.0049(3)
O_h4	0.88058(12)	0.32655(8)	0.02338(16)	0.01113(16)	0.0130(4)	0.0111(4)	0.0087(4)	−0.0030(3)	−0.0042(3)	0.0044(3)
O_w5	0.27352(12)	0.46268(9)	0.77494(17)	0.00907(14)	0.0099(3)	0.0085(4)	0.0089(3)	0.0008(3)	0.0011(3)	0.0009(3)
H_w1	0.311(3)	0.423(2)	−0.092(4)	0.008(6)						
H_w2	0.237(4)	0.536(3)	0.818(5)	0.009(6)						
H_h3	0.045(3)	0.380(2)	0.635(5)	0.010(6)						
H_h4	0.968(3)	0.281(2)	0.101(5)	0.009(6)						

The anisotropic displacement parameters are defined as: $\exp[-2\pi^2\Sigma_{i=1}^{3}\Sigma_{j=1}^{3}U_{ij}a_i^*a_j^*h_ih_j]$, U_{equiv} according to Ref. [10].

Table 3
Interatomic bond distances (Å) and bond angles (deg) for $M[PO_2(OH)_2]_2 \cdot 2H_2O$ compounds (M = Ni, Zn, Cd)

$M[PO_2(OH)_2]_2 \cdot 2H_2O$:	M = Ni		M = Zn		M = Cd	
Temperature (K):	295	*120*	295	*120*	295	*120*
M–O1, 2 ×	2.0752(10)	*2.0744(9)*	2.1014(9)	*2.0970(9)*	2.2674(10)	*2.2654(9)*
M–O2, 2 ×	2.0958(9)	*2.0964(9)*	2.1228(8)	*2.1248(9)*	2.2832(10)	*2.2847(10)*
M–O_w5, 2 ×	2.0779(10)	*2.0726(10)*	2.1186(9)	*2.1105(10)*	2.3240(11)	*2.3155(10)*
P–O1	1.5084(10)	*1.5109(10)*	1.5084(10)	*1.5104(9)*	1.5084(10)	*1.5113(9)*
P–O2	1.5085(10)	*1.5124(9)*	1.5085(10)	*1.5125(10)*	1.5085(10)	*1.5114(10)*
P–O_h3	1.5663(12)	*1.5666(10)*	1.5663(12)	*1.5655(10)*	1.5663(12)	*1.5649(10)*
P–O_h4	1.5691(10)	*1.5735(10)*	1.5691(10)	*1.5745(10)*	1.5691(10)	*1.5744(10)*
O1–P–O2	114.09(6)	*113.93(5)*	114.18(5)	*114.09(5)*	113.98(6)	*113.91(5)*
O1–P–O_h3	106.06(6)	*106.19(5)*	106.12(6)	*106.25(5)*	106.04(7)	*106.18(5)*
O1–P–O_h4	108.60(6)	*108.53(5)*	108.43(5)	*108.30(5)*	108.18(6)	*108.09(5)*
O2–P–O_h3	110.21(7)	*110.35(5)*	110.39(6)	*110.45(5)*	111.01(7)	*111.16(5)*
O2–P–O_h4	109.64(5)	*109.53(5)*	109.70(5)	*109.53(5)*	109.86(6)	*109.74(5)*
O_h3–P–O_h4	108.03(7)	*108.12(5)*	107.78(6)	*108.01(5)*	107.50(7)	*107.50(6)*

Low temperature data are shown in italics.

(Jahn–Teller effect; it was extensively discussed [13]). However, in $Co[PO_2(OH)_2]_2(H_2O)_2$ the distortion of the CoO_6 polyhedron is obviously not controlled by the electron configuration of the Co^{2+} ion. In most cases of the $M[PO_2(OH)_2]_2(H_2O)_2$ compounds, *M*–O_w5 are the longest bonds within the octahedra. Only exceptionally, for M = Ni and Zn, the *M*–O2 bonds are longer; it is somewhat unusual that the interatomic bond distances to an O_w atom are not the longest bonds within a coordination polyhedron. It might be enabled by the polarization of the P^{5+} ion within the *di*protonated $PO_2(OH)_2$ group. The compression of the $MO_4(O_w)_2$ octahedra from 295 to 120 K is extremely small and amounts for the average $\langle M\text{–O}\rangle$ bond lengths 0.002–0.003 Å; the largest compressibility for individual bond lengths were observed for *M*–O_w5.

Bond-distance (DI_d), bond-angle ($DI\angle$) and O–O-edge (DI_e) distortions were calculated for the MO_6 octahedra and the PO_4 tetrahedra according to Refs. [13,14]; they are compiled in Table 4. For the MO_6 octahedra, a positive correlation is observed between the distortion parameters and the ionic radii of the *M* atoms (Fig. 3b). The variation is small for the bond-distance distortions. A significant difference between the trend lines observed for the room-temperature and low-temperature data is observed only for the DI_d values.

3.3. $PO_2(OH)_2$ groups

The geometry of the *di*protonated phosphate groups are in accordance with general aspects outlined earlier [14,15]. The P–O bond lengths are 1.501–1.512 Å whereas P–O_h is 1.554–1.578 Å (Fig. 4a). The bond angles O1–P–O2 are significantly larger as compared to that of O–P–O_h and O_h–P–O_h (Fig. 4b). The single bond distances and bond angles are more or less constant within the complete series of compounds. The bond lengths are slightly increased for the low-temperature data as compared to the room-temperature structures; the bond angles are practically

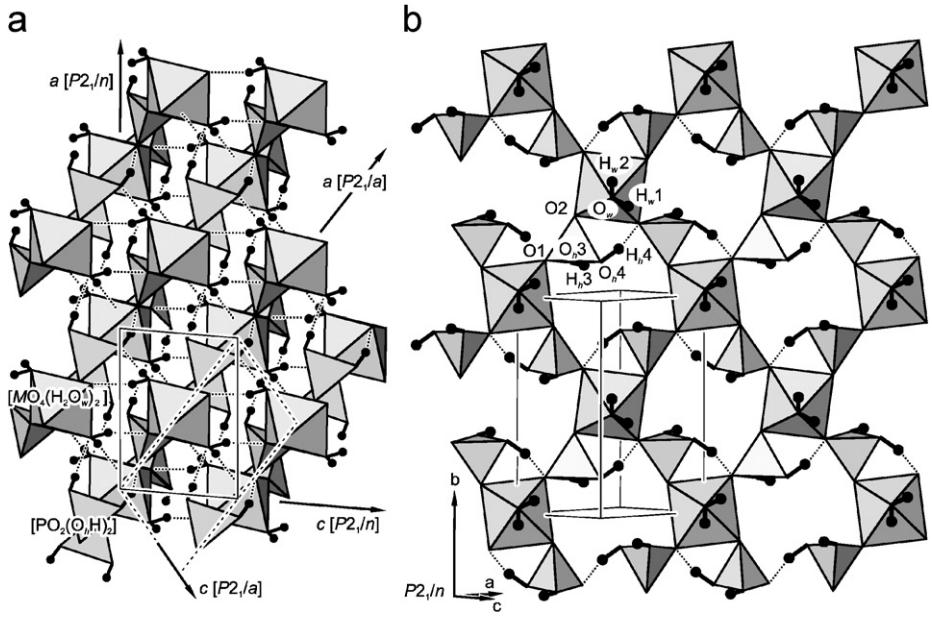

Fig. 1. The crystal structure of $M[PO_2(OH)_2]_2 \cdot 2H_2O$ compounds. (a) Projection parallel [010] showing the direction of a and c for different cell choices: the $P2_1/n$ cell is the reduced cell referring to the atomic coordinates given in Table 2. The $P2_1/a$ setting is used only for the explanation of the temperature-related compression behaviour with two crystallographic axes (a and b axes) within the $M[PO_2(OH)(O_h)_2]_2(O_w)_2$ layer and the third axes (c axis) inclining. (b) View of a $M[PO_2(OH)_2]_2(H_2O)_2$ layer; the axes directions are indicated for the $P2_1/n$ cell (programme ATOMS [11]).

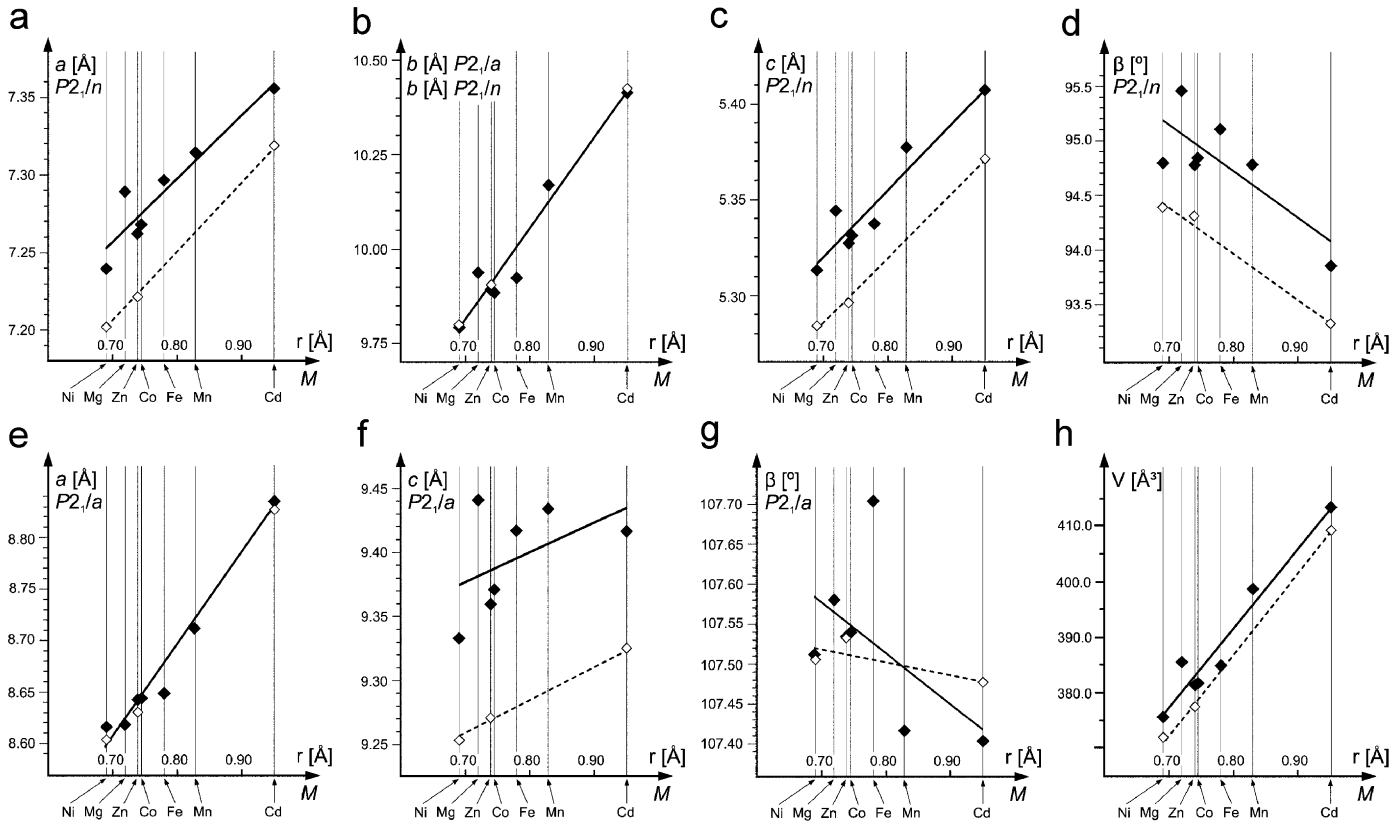

Fig. 2. Unit-cell parameters and cell volume of $M[PO_2(OH)_2]_2 \cdot 2H_2O$ compounds varying with the ionic radii r of the M atoms [12]. (a) Lattice parameter a, $P2_1/n$ setting; (b) lattice parameter b, $P2_1/n$ and $P2_1/a$ setting; (c) lattice parameter c, $P2_1/n$ setting; (d) monoclinic angle β, $P2_1/n$ setting; (e) lattice parameter a, $P2_1/a$ setting; (f) lattice parameter c, $P2_1/a$ setting; (g) monoclinic angle β, $P2_1/a$ setting; (h) volume of the unit cell. Room-temperature and low-temperature data are represented by full and empty diamonds, respectively. Their trend lines are shown as solid and broken lines; in (b) and (e) the trend lines overlap each other.

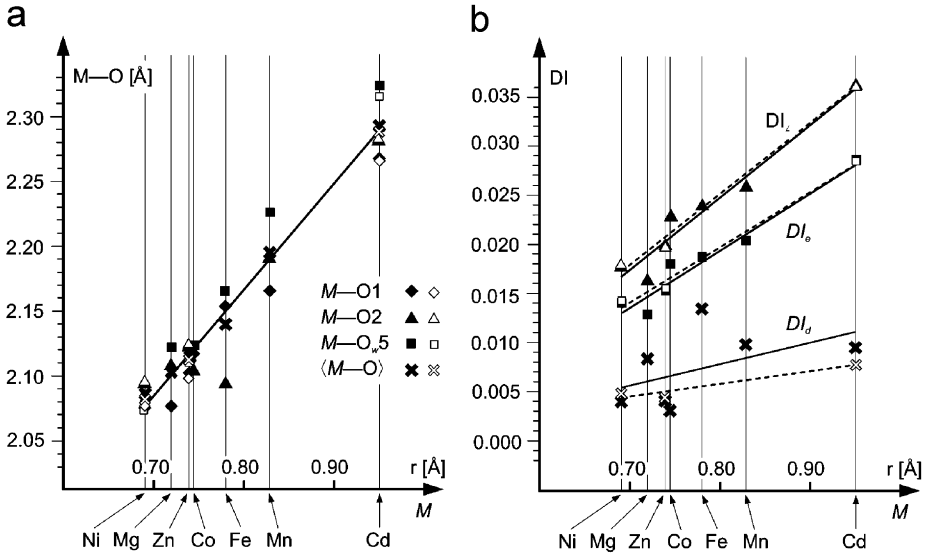

Fig. 3. The MO_6 octahedra within the $M[PO_2(OH)_2]_2 \cdot 2H_2O$ compounds: variation of (a) the M–O bond lengths and (b) the distortion parameters (for definition cf. Table 5) with the ionic radii r of the M atoms [12]. Room-temperature and low-temperature data are represented by full and empty symbols, respectively. Their trend lines are shown as solid and broken lines; in (a) both the trend lines overlap each other.

Table 4
Distortion parameters for the coordination polyhedra around the M and P atoms of $M[PO_2(OH)_2]_2 \cdot 2H_2O$ compounds (M = Mg, Mn, Fe, Co, Ni, Zn, Cd)

M	PO_4 tetrahedron			MO_6 octahedron		
	DI_d	$DI_\angle$	DI_e	DI_d	$DI_\angle$	DI_e
Mg [3]	0.0204	0.0192	0.0088	0.0084	0.0164	0.0128
Mn [4]	0.0198	0.0195	0.0091	0.0098	0.0259	0.0203
Fe [5]	0.0172	0.0173	0.0084	0.0134	0.0239	0.0187
Co [6]	0.0192	0.0181	0.0092	0.0030	0.0229	0.0180
Ni, 295 K (this work)	0.0193	0.0171	0.0086	0.0041	0.0180	0.0141
Ni, 120 K (this work)	0.0190	0.0167	0.0086	0.0048	0.0182	0.0142
Zn, 295 K (this work)	0.0195	0.0182	0.0091	0.0041	0.0197	0.0154
Zn, 120 K (this work)	0.0190	0.0175	0.0090	0.0044	0.0197	0.0155
Cd, 295 K (this work)	0.0201	0.0200	0.0093	0.0094	0.0361	0.0285
Cd, 120 K (this work)	0.0189	0.0199	0.0097	0.0079	0.0361	0.0283

The bond distance, bond angle and O–O edge distortions are defined as $DI_d = (\sum_{i=1}^{n1}|d_i - d_m|)/n_1 d_m$, $DI_\angle = (\sum_{i=1}^{n2}|\angle_i - \angle_m|)/n_2 \angle_m$ and $DI_e = (\sum_{i=1}^{n2}|d_e - d_e|)/n_2 d_e$, respectively.
d, $\angle$, e signify M–O/P–O bond distances, O–M–O/O–P–O angles and O–O edges within the relevant polyhedron; indexes i and m indicate individual and mean values for the relevant polyhedron $n1$ and $n2$ are 4 and 6 for the phosphate tetrahedron and 6 and 12 for the $MO6$ octahedron (cf. [14,13]).

maintained in the investigated temperature range. The bond distance, bond angle and O–O edge distortions are small. They are neither significantly influenced by the size of the $MO_4(O_w)_2$ octahedra nor by the temperature condition.

3.4. Hydrogen bonds

The geometries of the hydrogen bonds are compiled in Table 5 for the compounds investigated during the present work. In all cases, the hydrogen-bond lengths of the low-temperature measurements are smaller as compared with that at room temperature. The differences are approximately the same and the relevant trend lines are nearly parallel to each other (Fig. 5a). $O_h4\cdots O1$ is markedly shorter as compared with the three other hydrogen-bond lengths within this series of compounds and practically independent from the size of the M atoms (the only exception is M = Mg and to a smaller extent M = Mn). It is within the $M[PO_2(OH)_2]_2(H_2O)_2$ layer. The three other hydrogen bonds are less strong. They exhibit a significant influence by the size of the M atoms. Whereas $O_h3\cdots O_w5$ and $O_w5\cdots O2$ are negatively correlated with $r(M)$, $O_w5\cdots O_h4$ is positively correlated. Fig. 5b shows the variation of the $O\cdots O_w\cdots O$ bond angles.

Both atoms O1 and O2 are coordinated by each an M and a P atom; furthermore, they are acceptors of hydrogen bonds. The bond strength contribution of the hydroxyl groups O_h4–H_h4 and O_w5–H_w1 to their acceptor atoms O1 and O2 are distinct due to the different hydrogen-bond

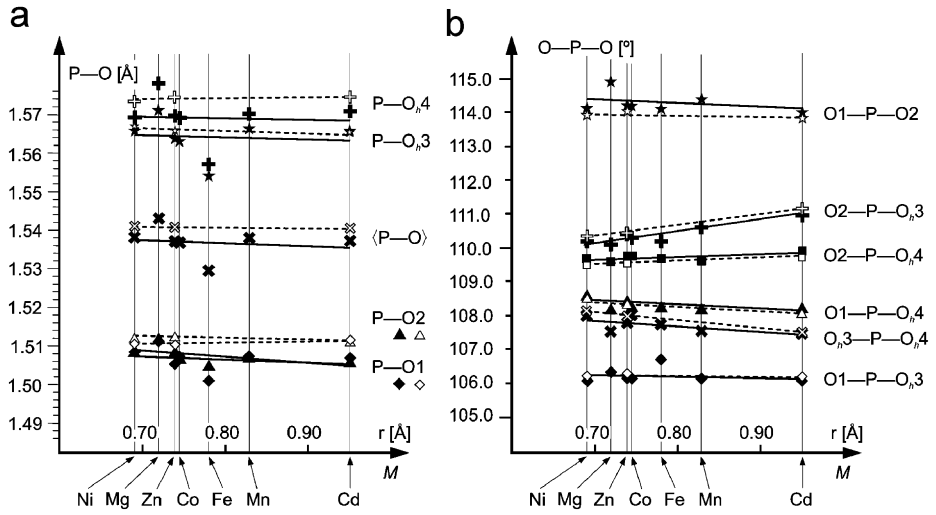

Fig. 4. The $[PO_2(OH)_2]_2$ groups within the $M[PO_2(OH)_2]_2 \cdot 2H_2O$ compounds: variation of (a) the P–O bond lengths and (b) the O–P–O bond angles with the ionic radii r of the M atoms [12]. Room-temperature and low-temperature data are represented by full and empty symbols, respectively. Their trend lines are shown as solid and broken lines.

Table 5
Hydrogen bonds: bond lengths in Å and bond angles in ° for $M[PO_2(OH)_2]_2 \cdot 2H_2O$ compounds (M = Ni, Zn, Cd)

Donor–H···acceptor	D···A	D–H	H···A	D–H···A	A···O$_w$···A′	H–O$_w$–H′
$Ni[PO_2(OH)_2]_2 \cdot 2H_2O$, 295 K						
O$_w$5–H$_w$1···O2	2.7300(14)	0.85(3)	1.90(3)	162(3)	82.67(4)	103(3)
O$_w$5–H$_w$2···O$_h$4	2.7060(15)	0.81(3)	1.96(3)	153(3)		
O$_h$3–H$_h$3···O$_w$5	2.7457(16)	0.64(3)	2.12(3)	165(3)		
O$_h$4–H$_h$4···O1	2.5735(14)	1.00(4)	1.61(4)	160(4)		
$Ni[PO_2(OH)_2]_2 \cdot 2H_2O$, 120 K						
O$_w$5–H$_w$1···O2	2.7102(13)	0.90(2)	1.84(2)	161(2)	83.48(4)	108(3)
O$_w$5–H$_w$2···O$_h$4	2.6878(13)	0.82(3)	1.94(3)	152(3)		
O$_h$3–H$_h$3···O$_w$5	2.7180(14)	0.71(3)	2.03(3)	164(3)		
O$_h$4–H$_h$4···O1	2.5602(13)	1.04(4)	1.58(5)	153(4)		
$Zn[PO_2(OH)_2]_2 \cdot 2H_2O$, 295 K						
O$_w$5–H$_w$1···O2	2.7212(13)	0.89(2)	1.86(2)	161(2)	81.16(4)	104(2)
O$_w$5–H$_w$2···O$_h$4	2.7129(13)	0.83(3)	1.94(2)	155(2)		
O$_h$3–H$_h$3···O$_w$5	2.7422(15)	0.67(2)	2.09(2)	166(3)		
O$_h$4–H$_h$4···O1	2.5846(13)	0.92(3)	1.74(3)	151(3)		
$Zn[PO_2(OH)_2]_2 \cdot 2H_2O$, 120 K						
O$_w$5–H$_w$1···O2	2.7012(14)	0.89(2)	1.84(3)	163(2)	85.03(4)	104(2)
O$_w$5–H$_w$2···O$_h$4	2.6928(13)	0.81(2)	1.92(2)	158(2)		
O$_h$3–H$_h$3···O$_w$5	2.7133(13)	0.70(2)	2.02(2)	167(2)		
O$_h$4–H$_h$4···O1	2.5690(13)	0.87(2)	1.75(3)	156(2)		
$Cd[PO_2(OH)_2]_2 \cdot 2H_2O$, 295 K						
O$_w$5–H$_w$1···O2	2.6946(16)	0.84(2)	1.87(2)	167(3)	92.58(5)	108(3)
O$_w$5–H$_w$2···O$_h$4	2.7399(16)	0.81(3)	1.96(3)	164(3)		
O$_h$3–H$_h$3···O$_w$5	2.7174(16)	0.66(3)	2.07(3)	166(3)		
O$_h$4–H$_h$4···O1	2.5772(14)	0.87(3)	1.73(3)	162(3)		
$Cd[PO_2(OH)_2]_2 \cdot 2H_2O$, 120 K						
O$_w$5–H$_w$1···O2	2.6769(15)	0.86(2)	1.83(2)	170(2)	93.34(4)	107(3)
O$_w$5–H$_w$2···O$_h$4	2.7226(14)	0.85(3)	1.89(3)	165(3)		
O$_h$3–H$_h$3···O$_w$5	2.6939(14)	0.72(2)	1.99(2)	170(3)		
O$_h$4–H$_h$4···O1	2.5642(13)	0.88(2)	1.71(2)	164(2)		

lengths. The crystal structure adopts for these differences with slightly longer M–O2 and shorter M–O1 bond distances; the same trend even to a smaller extent is observed for the P–O2 and P–O1 bonds, respectively. The M–O2–P angle is opposite of the O$_h$4···O1 hydrogen bond and forms *quasi* a triangle with the O1–O2 edge of an MO_6

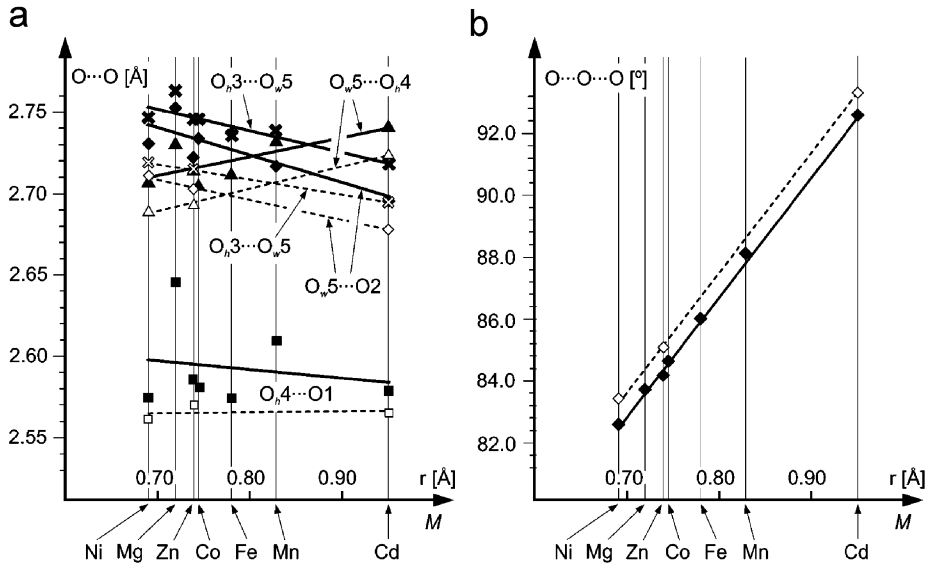

Fig. 5. Hydrogen-bond lengths and acceptor···O_w···acceptor angles of the water molecules within the $M[PO_2(OH)_2]_2 \cdot 2H_2O$ compounds: variation of (a) the O···O bond lengths and (b) the O···O_w···O bond angles with the ionic radii r of the M atoms [12]. Room-temperature and low-temperature data are represented by full and empty symbols, respectively. Their trend lines are shown as solid and broken lines.

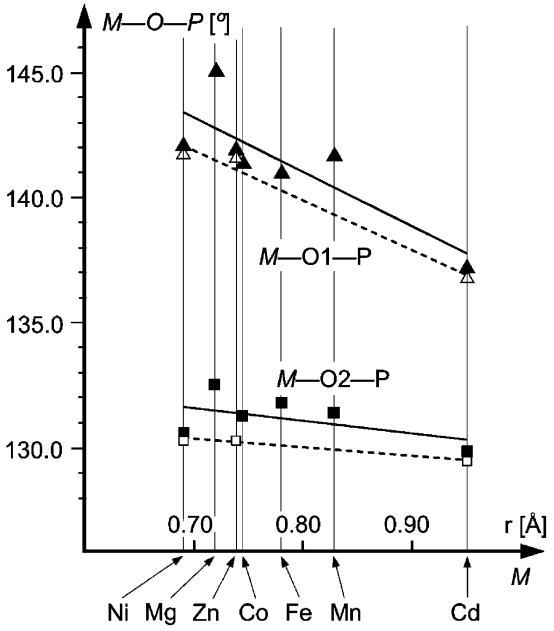

Fig. 6. The variation of the M–O–P bond angles within the $M[PO_2(OH)_2]_2 \cdot 2H_2O$ compounds with the ionic radii r of the M atoms [12]. Room-temperature and low-temperature data are represented by full and empty symbols, respectively. Their trend lines are shown as solid and broken lines.

octahedron and the O2–O_h4 edge of a $PO_2(OH)_2$ tetrahedron. This causes that the M–O2–P angles are smaller and less influenced by the size of the M atoms as compared to those of the M–O1–P angles (Fig. 6). The variation in the M–O1–P angles compensates for the size of the MO_6 octahedra.

The atoms O_h3 and O_h4 belonging to hydroxyl groups are within one $PO_2(OH)_2$ tetrahedron. Only the atoms O_h4 represent acceptors of a hydrogen bond. Like above, P–O_h3 is slightly smaller as compared to P–O_h4 to adopt for the contribution of the hydrogen bond to the bond valence sum.

4. Vibrational analysis of $M[PO_2(OH)_2]_2 \cdot 2H_2O$

4.1. Vibrations of the $H_2PO_4^-$ ions

The free PO_4^{3-} ion has T_d molecular symmetry, thus there are four normal modes of vibrations—$\nu_1(A_1)$ and $\nu_3(F_2)$ are symmetric and asymmetric stretching modes, respectively; $\nu_2(E)$ and $\nu_4(F_2)$ are symmetric and asymmetric bending modes, respectively. All of which are Raman active, but only the triple degenerated ν_3 and ν_4 modes are IR active. The presence of two P–O_h bonds in the $H_2PO_4^-$ anion causes a reduction of its molecular symmetry and the highest possible symmetry of $H_2PO_4^-$ is C_{2v}. As a result, the degeneracy of the modes ν_2, ν_3 and ν_4 is removed: ν_2 splits into two components ($A_1 + A_2$) and both ν_3 and ν_4 into three components ($A_1 + B_1 + B_2$). Because of the intra-ionic coupling for the PO_4 stretching vibrations (two longer P–O_h and two shorter P–O bonds), the four stretching modes may be regarded as ν_s(P–O_h), ν_{as}(P–O_h), ν_s(P–O) and ν_{as}(P–O) in order of increasing frequencies [16,17]. In addition to the nine internal PO_4 vibrations, six vibrations involving OH motions are characteristic for $H_2PO_4^-$, namely: ν_{OH}, δ_{OH} and γ_{OH} for each OH bond (i.e., stretching O–H, in-plane and out-of-plane bending P–O–H vibration); this gives in total 15 fundamentals for $H_2PO_4^-$.

Due to the lower C_1 site symmetry of $H_2PO_4^-$ in the $M[PO_2(OH)_2]_2 \cdot 2H_2O$-type crystal lattice, all normal modes being of A-type symmetry become IR allowed. Additionally, each vibration mode could undergo factor-group splitting into four components ($A_u + A_g + B_u + B_g$),

where "*u*" species are IR active and "*g*" species are Raman active (C_{2h} factor-group symmetry). Thus, 8 and 10 bands corresponding to the stretching and bending PO_4 vibrations, respectively, are expected to appear in the IR spectra of $M[PO_2(OH)_2]_2 \cdot 2H_2O$.

The IR spectra of the $M[PO_2(OH)_2]_2 \cdot 2H_2O$ compounds are presented in Fig. 7. All spectra are similar in the regions of the stretching and bending PO_4 vibrations (1200–800 and 600–350 cm^{-1}, respectively) as well as in the high-frequency region of the hydrogen-bond motions (3500–1200 cm^{-1}), originating from both the P–OH conformation and the water molecule. The assignment of the bands in the IR spectra of the $M[PO_2(OH)_2]_2 \cdot 2H_2O$ compounds (see Table 6) is based on the spectroscopic data for different *di*- and *mono*-hydrogen phosphates [16–25]. Thus, the strong band at about 945–975 cm^{-1} is attributed to the stretching vibration of the longer P–O_h bonds, whereas the (three or four) bands at the higher frequency range of 1030–1180 cm^{-1} to the stretching vibrations of the shorter P–O bonds. The band at about 900 cm^{-1} could contribute both ν(P–O_h) and γ_{OH} modes. The bending vibrations O–P–O are expected to appear in the 350–600 cm^{-1} region. The less intensive band in the range 350–420 cm^{-1} more probably originates from the symmetric bending mode O–P–O. The stronger absorption bands between 450 and 560 cm^{-1} are due to the asymmetric bending vibrations O–P–O. However, one of the librational modes of the water molecule may overlap (see below). Thus, the smaller number of the bands observed in the IR spectra than theoretically allowed shows that the predictions arising from the factor group analysis are not completely fulfilled. It is evident that the band frequencies of the PO_4 vibrations are not essentially affected by the nature of the M^{2+} ions. The mean values of the stretching vibrations PO_4 appear within the series at almost the same wavenumbers (1025–1030 cm^{-1}); no systematic correlation between the wavenumbers and the size or the electronic configuration of M^{2+} is observed. Only in the Mg salt the P–O stretching modes are shifted to higher frequencies (mean value 1047 cm^{-1}). This upshift could be related to the more ionic nature of the Mg–O bonds compared with the *M*–O bonds of the other metal ions (a strengthening of the intra-molecular P–O bonds owing to the weakening of the inter-molecular Mg–O bonding [26,27]).

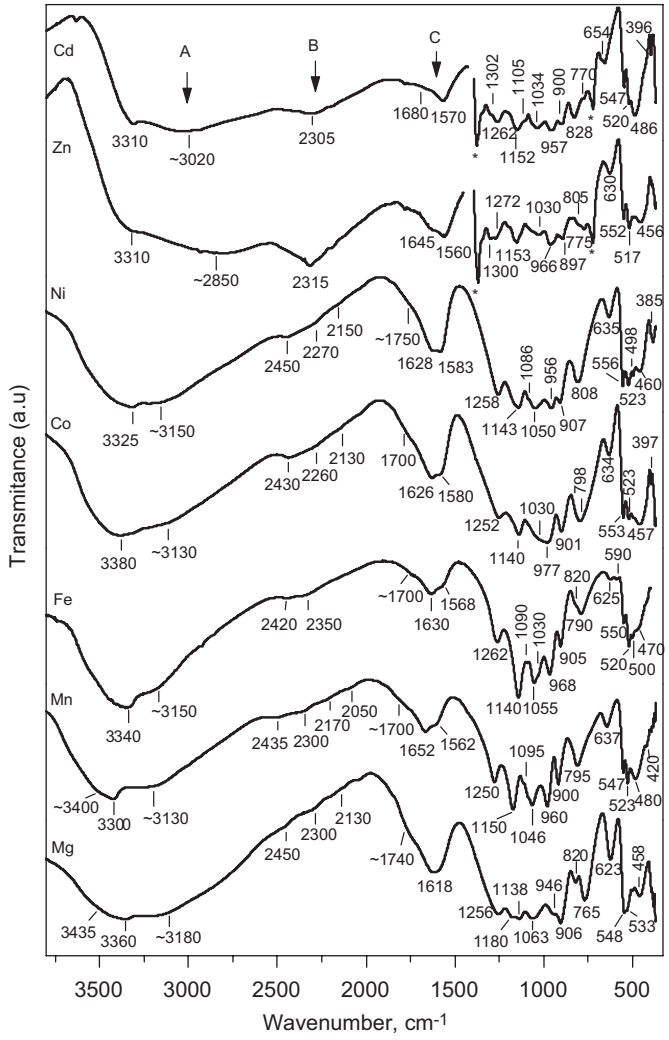

Fig. 7. IR spectra of $M[PO_2(OH)_2]_2 \cdot 2H_2O$ (KBr discs for M = Mg, Mn, Fe, Co and Ni; Nujol (1400–350 cm^{-1}) and Flurolube (4000–1400 cm^{-1}) mulls for M = Zn and Cd; * nujol bands).

From the site-group approximation of the OH group vibrations, two δ_{OH} and two γ_{OH} bands are expected (but twice more according to the factor-group analysis). The δ_{OH} mode gives rise to one or two bands (in the Zn and Cd salts) at 1250–1300 cm^{-1}. The band observed in all spectra between 795 and 830 cm^{-1} is assigned to the γ_{OH} mode. The second band around 765–790 cm^{-1} found in the IR spectra of the Mg, Fe, Zn and Cd salts could be due to γ_{OH} and/or the water-librational mode.

It is known that the existence of short O–H···O hydrogen bonds (with O···O distances between 2.45 and 2.65 Å) in a variety of strong hydrogen bonded solids is manifested by the formation of the characteristic "*ABC*" structure of the ν_{OH} vibrational bands [21–25,28–31]. One of the most popular interpretations of the *ABC* trio suggests a strong Fermi resonance between the ν_{OH} stretching modes and the overtones or combinations involving the bending δ_{OH} and γ_{OH} vibrations [32]. Usually, the triple *ABC* bands are very broad and consist of many ill-resolved components (*A* is located in the region of about 2900–2700 cm^{-1}, it is the strongest band; *B* is about 2600–2400 cm^{-1} and *C* around 1600–1700 cm^{-1}). The band *A* is very sensitive to the O···O distance; it is shifted to lower frequencies for decreasing hydrogen-bond lengths. Simultaneously, the intensity of *A* decreases, whereas the intensities of the *B* and *C* bands increase [33,34].

The characteristic *ABC* trio is clearly seen in the IR spectra of the $M[PO_2(OH)_2]_2 \cdot 2H_2O$ compounds (Fig. 7). In all spectra band *A* is strongly asymmetric at the low-frequency side with a smoothly diminishing intensity. Because of the overlap of band *A* with the ν_{OH} stretching modes of the water molecule, its frequency cannot be

Table 6
Assignments of the bands in the IR spectra of $M[PO_2(OH)_2]_2 \cdot 2H_2O$

M = Mg	M = Mn	M = Fe	M = Co	M = Ni	M = Zn	M = Cd	Assignments
3435 sh 3360	3400 sh 3300	3340	3380	3324	3310	3310	ν_{OH} (H_2O)
~3170	~3130	~3150	~3130	~3150	~2850	~3020	A band
2450 2300 2130	2435 2300 2170 2050	2420 2350	2430 ~2260 ~2130	2450 ~2270 ~2150	2315	2305	B band
1740 sh 1618	1760 sh 1652 1562 sh	1700 sh 1630 1568	1700 sh 1626 1580	1760 sh 1628 1583	1645 sh 1560	~1680 1570	C band and δ_{H_2O}
1256	1250	1262	1252	1258	1300 1272	1302 1262	δ_{OH}
1180 1138 1063	1150 1095 sh 1046	1142 1090 1055 1030 sh	1140 1080 sh 1030 sh	1143 1086 sh 1050	1153 1070 sh 1030	1152 1105 sh 1070 sh 1034	ν(P–O)
946	960	968	977	956	966	957	ν(P–O_h)
906	900	905	901	907	897	900	ν(P–O_h) and/or γ_{OH}
820	795	820	798	808	805	828	γ_{OH}
765		790			775	770	γ_{OH} and/or ν_L (H_2O)
623	637	625 590	634	635	630	654	ν_L (H_2O)
548 533 sh 458	547 523 480	550 520 500 470	553 523 520 457	556 523 498 460	552 517 456	547 520 486	δ_{as} (OPO)
	420 sh		397	385		396	δ_s (OPO)

measured precisely. The maximum of band *A* is approximately between 3130 and 3180 cm^{-1} in the Mn, Co, Fe, Ni salts, and around 3000 and 2850 cm^{-1} in Cd and Zn salts, respectively. Band *B* is observed also as a broad asymmetric band with several ill-resolved maxima between 2050 and 2450 cm^{-1}. Band *C* can be found around 1600–1700 cm^{-1}. However, the bending mode of the water molecule appears in the same frequency range. So, the complex absorption with maxima between 1550 and 1740 cm^{-1} contributes both to the band *C* and to the water bending mode. In all spectra the "*AB*" and "*BC*" gaps are observed at 2500 and 1900 cm^{-1}, respectively. Only in the Mg salt, there is no clear "*AB*" gap.

According to the crystal-structure investigations, the $M[PO_2(OH)_2]_2 \cdot 2H_2O$ compounds exhibit rather different hydrogen-bond lengths for their two hydroxyl groups (Fig. 5a). The intra-layer hydrogen bond $O_h4{-}H_h4\cdots O1$ varies within the series of compounds from 2.573 to 2.609 Å (with exception of the Mg salt, where it is as long as 2.645 Å); thus they are in the upper limit of the so-called strong hydrogen bonds (O···O bond lengths within the range from 2.40 to 2.60 Å; [29]). However, if the *inter*-layered $O_h3{-}H_h3\cdots O_w5$ hydrogen bond is longer (between 2.72 and 2.76 Å), it is classified as intermediate [29]. Obviously only the short O_h4–$H_h4\cdots O1$ hydrogen bond is responsible for the creation of the *ABC* trio in the $M[PO_2(OH)_2]_2 \cdot 2H_2O$ compounds. The correlation curves between the *A* band frequency and O–H···O bond lengths in some hydrogen phosphates, -sulphates, -arsenates and -selenites were found to be similar [34,35]. From the correlation curves thus proposed for the given O···O distances of about 2.57–2.60 Å, the band *A* is expected to appear around 2800 cm^{-1} or even below. Actually, in all $M[PO_2(OH)_2]_2 \cdot 2H_2O$ compounds studied, band *A* is shifted to higher wavenumbers by about 200–300 cm^{-1}. These findings provide evidence, that the hydrogen bond O_h4–$H_h4\cdots O1$ is less strong than deduced from its bond distance. The O_h4 atom is simultaneously an acceptor atom of a hydrogen bond from the water molecule (O_w5–$H_w2\cdots O_h4$); it might influence the observed weakening (Fig. 1b and Table 5). The overtones $2\delta_{OH}$ and $2\gamma_{OH}$ should be expected in the regions of 2600–2450 and

1800–1600 cm^{-1}, respectively. However, the ν_{OH} stretching fundamental (about 3100 cm^{-1}) is relatively far from the $2\delta_{OH}$ and $2\gamma_{OH}$ frequencies. As a consequence, the Fermi resonance is weak which could explain the high intensity of the *A* band and the low intensity of the *B* band as well as the relatively large difference between the wavenumbers of the *A* and *B* bands (about 700 cm^{-1}).

4.2. Vibrations of the water molecule

The water molecule in the $M[PO_2(OH)_2]_2 \cdot 2H_2O$ compounds has site symmetry C_1 and forms two different hydrogen bonds with bond lengths of 2.704–2.752 Å (Fig. 5a). The broad band with one or two maxima at 3300–3450 cm^{-1} (Fig. 7) is attributed to the stretching vibrations of the water molecule. The corresponding bending vibration δ_{H_2O} together with the band *C* gives rise to the broad band between 1500 and 1800 cm^{-1}.

The analysis of the spectroscopic data evidences that within the isotypic series the O–H stretching modes of the water molecule are slightly shifted to lower wavenumbers in the order $M = Mg > Mn \approx Fe \approx Co > Ni > Zn \approx Cd$ (Fig. 7, Table 6). The observed downshift could be correlated with the influence of the two factors: (i) the change in the character of the M–O_w interactions from more ionic in the Mg salt to more covalent in the cases of the Zn and Cd compounds, and (ii) with the increasing M–O_w interactions (synergetic effect [36]) in the order $Mn < Fe < Co < Ni$ as shown by the shortening of the respective M–O_w bonds in the same order (Fig. 3a).

One set of the three water librations (wagging, rocking, twisting—all IR allowed for C_1 site symmetry) is expected to appear in the IR spectra of $M[PO_2(OH)_2]_2 \cdot 2H_2O$. In crystalline hydrates the librational modes are normally observed in the region from 350 to 900 cm^{-1} and, thus they are often overlapped by the internal modes of the polyatomic ions ([36] and references therein). In the $M[PO_2(OH)_2]_2 \cdot 2H_2O$ compounds only the band at about 625–650 cm^{-1} observed in all spectra and the second one at 590 cm^{-1} found in the Fe salt can be unambiguously assigned to the water librations. The other librations should fall in the regions of the γ_{OH}, stretching and bending PO_4 vibrations.

Acknowledgments

Dr. V. Koleva is indebted to the National Science Fund of Bulgaria (Contract BM 1/2006) for financial support. The constructive remarks of the reviewers improved the manuscript; they are acknowledged with thanks.

References

[1] M.T. Averbuch-Pouchot, A. Durif, J.C. Guitel, I. Tordjman, M. Laügt, Bull. Soc. fr. Minér. Crist. 96 (1973) 278.
[2] M.T. Averbuch-Pouchot, J. Appl. Crystallogr. 7 (1974) 511.
[3] T.R. Hinsch, N. Jahrb. Miner. Mh. 1985 (1985) 439.
[4] P. Vasić, B. Prelesnik, M. Čurić, R. Herak, Z. Krist. 173 (1985) 193.
[5] W. Guse, K.H. Klaska, H. Saalfeld, G. Adiwidjaja, N. Jahrb. Miner. Mh. 1985 (1985) 433.
[6] H. Effenberger, Acta Crystallogr. C 48 (1992) 2104.
[7] A. Riou, Y. Cudennec, Y. Gerault, Acta Crystallogr. C 43 (1987) 194.
[8] A.J.C. Wilson (Ed.), International Tables for Crystallography, vol. C, Mathematical, Physical and Chemical Tables, Kluwer Academic Publishers, Dordrecht, Boston, London, 1992, p. 883.
[9] G.M. Sheldrick, SHELXL-97, a program for the refinement of crystal structures, University Göttingen, Germany, 1997.
[10] R.X. Fischer, E. Tillmanns, Acta Crystallogr. C 44 (1988) 775.
[11] E. Dowty, ATOMS: a computer program for displaying atomic structures, Shape Software, 521 Hidden Valley Road, Kingsport, TN, 2000.
[12] R.D. Shannon, Acta Crystallogr. A 32 (1976) 751.
[13] M. Wildner, Z. Krist. 202 (1992) 51.
[14] W.H. Baur, Acta Crystallogr. B 30 (1974) 1195.
[15] G. Ferraris, G. Ivaldi, Acta Crystallogr. B 40 (1984) 1.
[16] V. Videnova-Adrabińska, W. Wojciechowski, J. Baran, J. Mol. Struct. 156 (1987) 15.
[17] I. Hubert Joe, V.S. Jayakumar, G. Aruldhas, J. Solid State Chem. 120 (1995) 343.
[18] B. Marchon, A. Novak, J. Chem. Phys. 78 (1983) 2105.
[19] A. Bertoluzza, M.A. Battaglia, S. Bonora, P. Monti, R. Simoni, J. Mol. Struct. 127 (1985) 35.
[20] V. Videnova-Adrabińska, J. Baran, J. Mol. Struct. 175 (1988) 295.
[21] J. Xu, D.F.R. Gilson, I.S. Butler, Spectrochim. Acta A 54 (1998) 1869.
[22] L.B. Taher, L. Smiri, A. Bulou, J. Solid State Chem. 161 (2001) 97.
[23] T. BenChaabane, L. Smiri, A. Bulou, Solid State Sci. 6 (2004) 197.
[24] I. Němec, Z. Macháčková, K. Teubner, I. Císařová, P. Vaněk, Z. Mička, J. Solid State Chem. 177 (2004) 4655.
[25] J. Baran, T. Lis, M. Drozd, H. Ratajczak, J. Mol. Struct. 516 (2000) 185.
[26] H.D. Lutz, H. Haeuseler, Trends Appl. Scpectrosc. 2 (1998) 79.
[27] H.D. Lutz, J. Himmrich, M. Schimdt, J. Alloys Compounds 241 (1996) 1.
[28] D. Hadži, Pure Appl. Chem. 11 (1965) 435.
[29] A. Novak, Struct. Bonding 18 (1974) 177.
[30] V. Videnova-Adrabińska, J. Baran, J. Mol. Struct. 156 (1987) 1.
[31] M.K. Marchewka, J. Baran, Spectrochim. Acta A 60 (2004) 201.
[32] D. Hadži, S. Bratos, in: The Hydrogen Bond, vol. 2, North-Holland, Amsterdam, 1976, p. 565.
[33] S.E. Odinokov, A.V. Iogansen, Spectrochim. Acta A 28 (1972) 2343.
[34] K. Unterderweide, B. Engelen, K. Boldt, J. Mol. Struct. 322 (1994) 233.
[35] B.K. Choi, M.N. Lee, J. Raman Spectrosc. 20 (1989) 11.
[36] H.D. Lutz, Struct. Bonding (Berlin) 69 (1988) 97.